A facile method to observe graphene growth on copper foil

Fan Yang, Yangqiao Liu, Wei Wu, Wei Chen, Lian Gao and Jing Sun

State Key Laboratory of High Performance Ceramics and Superfine Microstructure, Shanghai Institute of Ceramics, Chinese Academy of Sciences, Shanghai 200050, People's Republic of China

E-mail: yqliu@mail.sic.ac.cn and jingsun@mail.sic.ac.cn

Abstract
A novel scanning electron microscope (SEM) method is presented for high contrast identification of each layer of pyramidal graphene domains grown on copper. We obtained SEM images by combining the advantages of the high resolution property of the secondary electron signal and the elemental sensitivity of the backscattering electron signal. Through this method, we investigated the difference in the growth mechanisms of mono-layer and few-layer graphene. Due to different lattice mismatches, both the surface adsorption process and the epitaxial growth process existed under the atmospheric growth conditions. Moreover, the copper oxidation process can be easily discovered. It is obvious from the SEM images that the graphene greatly delayed the oxidation process of the copper surface. Finally, the nucleation and growth speed of graphene domains was found to depend on the linear array distribution of surface ledges and terraces of annealed rolled copper foil. This result explains the linear rows of graphene during the growth process and accords with theoretical results.

S Online supplementary data available from stacks.iop.org/Nano/23/475705/mmedia

(Some figures may appear in colour only in the online journal)

1. Introduction

Graphene is an ideal candidate for a wide range of applications, especially in the electronic field [1, 3, 19, 38], due to its superb properties. Among various synthesis methods [6, 13, 21, 30, 31], the chemical vapor deposition (CVD) technique has demonstrated its potential application for large-area flexible touch screens [1, 14] already. In contrast to the surface adsorption mechanism in low pressure chemical vapor deposition [21–24, 36] (LPCVD), graphene growth under atmospheric pressure chemical vapor deposition (APCVD) is more complicated due to different kinetics [2]. Inhomogeneous graphene domains grown on copper foil are commonly reported [2, 41]. The relationship between the natural surface unevenness of the copper foil and the graphene growth remains obscure. To probe into its deep mechanism, it is imperative to develop an intuitive and efficient tool to characterize the few-layer graphene directly on the copper substrate.

Imaging techniques for graphene-based materials have been studied widely and deeply in recent years [18]. For CVD graphene on a catalyst, among various techniques, Raman mapping is relatively low in resolution while atomic force microscopy (AFM) is highly sensitive to substrate topography. Other tools are either unsuitable to characterize graphene on a catalyst, such as transmission electron microscopy (TEM), or not commonly used, such as low energy electron microscopy (LEEM). As a convenient general imaging method, a scanning electron microscope (SEM) is often adopted to measure the shape and distribution of graphene domains directly on a catalyst substrate [2, 35] but it has not been utilized for characterizing the number of graphene layers. In this paper, we present a systematic analysis of a novel SEM method which can image graphene layers directly on copper foil. The method provides immediate feedback in investigation of graphene growth. Through this versatile imaging method, we revealed different mechanisms of few-layer graphene domain growth and observed a copper oxidation process occurring at the interlayer between the graphene domains and the

copper foil. Moreover, we found for the first time that the inhomogeneous distribution of ledges and terraces on the catalyst surface strongly affects the growth tendency of the graphene domains.

2. Experimental details

2.1. Sample preparation

Graphene was grown on copper foil by APCVD, using methane as the carbon source. 25 μm thick copper foil (Alfa Aesar 13382#) was placed in a 3 inch quartz tube furnace. Firstly, the raw copper foil was annealed under H_2 atmosphere for 20 min at a temperature of 1000 °C. Then a mixture of methane, hydrogen and argon gases flowed in for 200 and 270 s to obtain isolated graphene domains (S_{IG}) and continuous graphene (S_{CG}) on copper foil, respectively. The flow rates of the mixed gases were 3.5 ml min^{-1} of methane, 20 ml min^{-1} of hydrogen and 1300 ml min^{-1} of argon, respectively. A large flow of the carrier gas argon was used to remove excessive activated carbon atoms. Then the sample was cooled down rapidly to room temperature in about 10 min.

2.2. Characterization techniques

The morphology of the graphene domains grown on copper was observed by a field-effect scanning electron microscope (Hitachi S-4800) and an atomic force microscope (Veeco Innova) in the tapping mode. The Raman signals including spectra and mapping were collected using a Raman microscope (Thermo Scientific Raman DXR) with an excitation length of 532 nm. X-ray photoelectron spectroscopy analysis was conducted using an Al Kα (1486.4 eV) monochromatic x-ray source (Axis Ultra DLD, Kratos).

3. Results and discussion

Previous [2, 35] CVD graphene characterization by SEM was conducted by collecting secondary electron (SE) signals, since this technique is highly morphology sensitive, with a penetration depth of secondary electrons of about 5–10 nm. However, the obtained images of the graphene domains are always obscure. It has been reported before that the number of graphene layers on a Si/SiO$_2$ substrate can be determined by SE signals with a lower accelerating voltage [15, 20]. However, this method is not suitable for graphene directly on catalyst because of the low contrast differences among graphene layers and the indistinct layer border [20]. The obtained SE mode image of sample S_{IG} directly on copper in figure 1(a) could hardly demonstrate the exact number of graphene layers, especially the few-layer part. We noticed that the substrate we use is an excellent electrical conductor which is suitable for collecting backscattering electron (BSE) signals [18]. By adding 15% of BSE signals, we obtained the SEM image shown in figure 1(b), which amazingly

reveals clearly various contrasts. We tried other percentages of BSE signal and found that the contrasts of the obtained SEM images were different, as shown in figure S1 in the supporting information (available at stacks.iop.org/Nano/23/475705/mmedia). We attribute this to the different penetration depths between the SE signal and the BSE signal. 15% of BSE signal is the optimal condition to observe graphene domains. Several contrasts stack layer by layer as a pyramid shape, just as reported [35] before. We assumed that these contrasts represent the number of graphene layers. To verify the number of graphene layers, we present G peak and 2D peak Raman mapping data in figures 1(c) and (d), respectively. All Raman mappings of graphene were characterized directly on copper foil. The characteristic G peak of graphene [7, 9] at ~1580 cm^{-1} represents sp^2 structure, and the 2D peak at ~2700 cm^{-1} demonstrates the number of graphene layers. The disorder induced D peak positioned at 1350 cm^{-1} shown in figure S2(a) (available at stacks.iop.org/Nano/23/475705/mmedia) is only stimulated at domain edges [41] and nucleation sites, indicating a high-quality growth process. We extracted several typical peaks of mapping data in figure 1(f) to demonstrate our assumption. For the lightest contrast area, point 1 in figure 1(b), the corresponding intensity of the 2D peak (I_{2D}) is more than twice that of the G peak (I_G) with a full width at half maximum (FWHM) of about 25 cm^{-1}, indicating mono-layer graphene. Meanwhile at darker contrast areas, point 2, I_{2D}/I_G decreases to ~1, which is the sign of bi-layer graphene. Point 3 is in the center of the domain where the contrast is the deepest. I_{2D}/I_G further decreases to less than 0.5. The FWHM of the 2D peak is about 67 cm^{-1}, demonstrating three-layer graphene. This accordance between contrast difference and Raman mapping result evidenced that the present mixed SE/BSE mode SEM method can clearly discriminate the exact graphene layer numbers [5]. In order to characterize the relationship between the contrasts in SEM and the exact layers of the graphene domain more precisely, we endeavored to find proper AFM data in the same region. However, the pyramidal shape cannot be easily seen due to the large altitude differences on the copper foil, as shown in figure S3(a) (available at stacks.iop.org/Nano/23/475705/mmedia). However, when transferred to a Si/SiO$_2$ substrate, the morphology of the graphene domains can be observed clearly by AFM characterization, as shown in figure S3(b) (available at stacks.iop.org/Nano/23/475705/mmedia). The AFM result is consistent with layer-by-layer stacking of pyramidal graphene evidenced by the SEM contrasts and Raman analysis discussed above.

By analyzing the gray scale histogram of each distinct contrast of over 50 SEM images using Photoshop software, we extracted the average value via the normal distribution and obtained the average contrast difference between two mode images curves in figure 1(e). First of all, we can see clearly that the slope is obviously higher using the mixed signal than for the SE signal. The contrast variance between adjacent layers is about five times larger in the mixed mode images. This provides further evidence of the large advantage of the mixed signal for the observation of CVD graphene on copper. From the point of view of
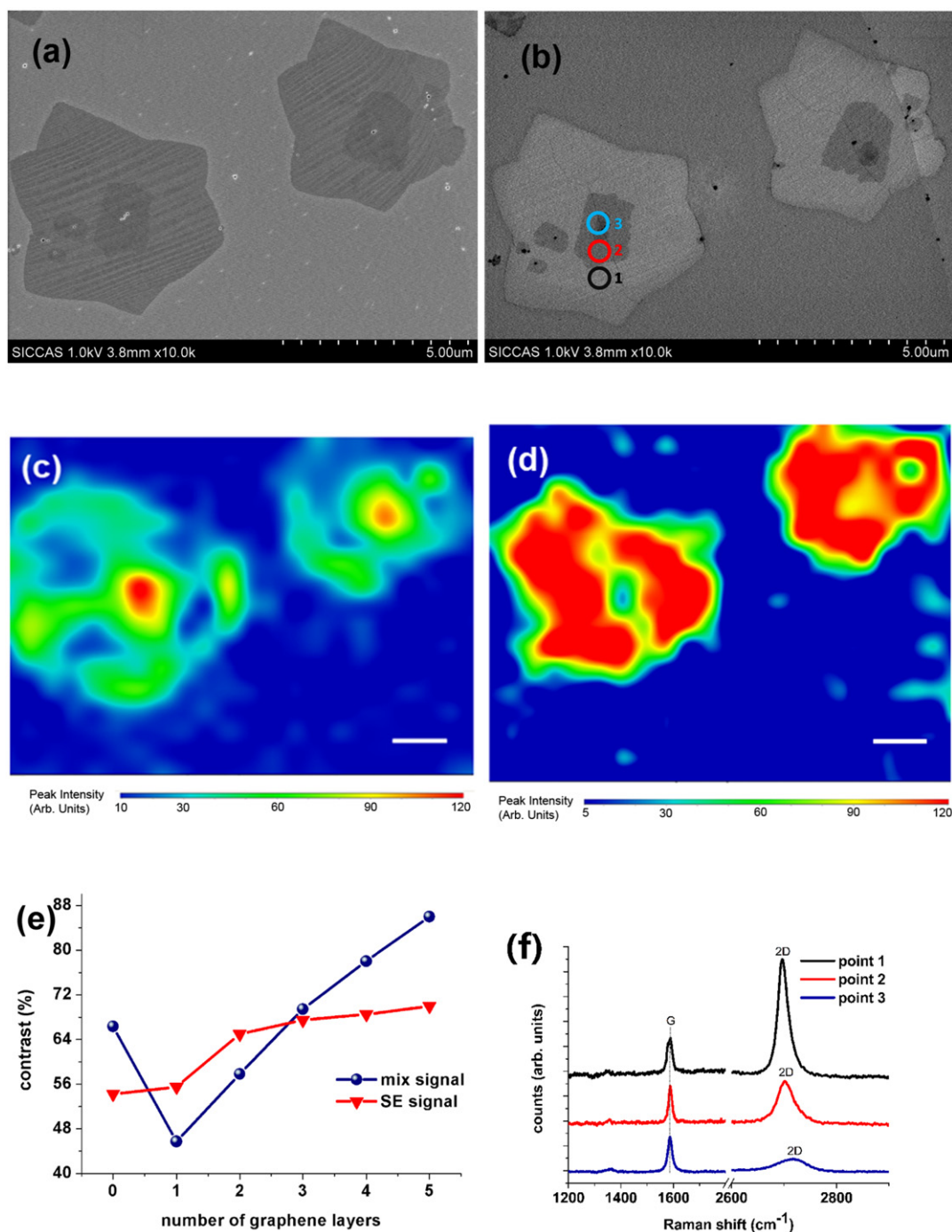
Figure 1. SEM images of isolated few-layer graphene domains of (a) the SE mode and (b) the mixed SE/BSE mode, respectively. (c), (d) Illustrate Raman mapping of the G peak and 2D peak respectively (scale bar 1 μm). (e) Exhibits curves of average contrast difference between two mode images. (f) Shows the Raman spectra of different points in the SEM image in (b).

the SEM technique [34], other than the morphology, the mean atomic number is the key for exhibiting clearly the exact number of graphene layers [11]. Although reflecting deeper ($\sim$50 nm) information, BSE signals, originated by elastically scattered electrons, vary sensitively with atomic number. As the number of graphene layers increases, the mean atomic number decreases accordingly, which results in a lower electron yield and thus a darker contrast in the image. Even if there is one layer increase or decrease of the

graphene layer, the contrast will be altered. Besides the BSE contribution, SE guarantees images exhibiting surface details clearly in focus. Moreover, the copper catalyst substrate possesses excellent conductivity which is perfectly suitable for collecting signals [18]. Therefore, clear surface details with varying number of graphene layers can be obtained by SEM. We found that the contrast difference between adjacent layers is almost the same. The contrast difference is reduced slightly when the number of graphene layers increases. Our

results fit the empirical formula [11] of the electron field of BSE signals.

Besides the pyramidal shape, we noticed that, no matter what shape the mono-layer graphene domains were, the upper few-layer graphene always followed a hexagonal shape (see figure S4 available at stacks.iop.org/Nano/23/475705/mmedia). We attribute this to different mechanisms between mono-layer graphene growth and upper few-layer graphene growth. It was already known [22] that mono-layer graphene grows by a surface adsorption process using LPCVD. On a copper substrate, activated carbon atoms migrate, nucleate and grow up to form mono-layer graphene. However, under atmospheric conditions, more collision activation occurs. Therefore, the residence time of activated carbon atoms becomes much longer, which results in a few-layer growth process. For few-layer graphene growth, the growth process is an epitaxial growth deposition process [28] since the growth substrate is changed to graphene where the lattice mismatch changes from 3.72% on copper [27] to 0 on mono-layer graphene. The deposited activated carbon atoms take on a lattice structure, whose orientation is identical to the substrate and follows a hexagonal shape growth. This is different from other thin-film deposition methods. In the process of thin-film growth [8, 29], the formation energy (E_f) and migration energy (E_m) of adatoms are not the same for mono-layer graphene and epitaxial graphene growth for different growth substrates. E_f and E_m of the adatoms are lower on copper than graphene substrate, leading to a faster speed for mono-layer graphene growth. This is verified by figure 1(b) in which the mono-layer graphene region is far larger than the epitaxial graphene. For epitaxial graphene growth, the growth speed is the same for each graphene layer due to the same dynamic effect.

Besides distinct contrasts, an odd phenomenon in figure 1(b) is that the copper substrate exhibits a darker contrast while the mono-layer graphene regions are much lighter. Also, the curves in figure 1(e) fit the empirical curves of electron yield in SE and BE signals except for the bare copper substrate. We extracted the Raman mapping of the CuO peak [4] at $\sim$290 cm^{-1} in figure S2(b) (see supplementary data available at stacks.iop.org/Nano/23/475705/mmedia). The peak can be found on the bare copper foil region without graphene coverage. We attributed this to an oxidation process on the copper surface which led to a lower mean atomic number. Figures 2(a) and (b) show isolated mono-layer graphene by collecting SE and mixed SE/BSE modes, respectively. Similarly to figure 1(b), the copper substrate in figure 2(b) exhibits a darker contrast than the mono-layer graphene region. Figures 2(c) and (d) illustrate XPS curves [4] of copper and carbon using S_{IG} and S_{CG} samples. S_{IG} refers to isolated graphene domains that partially coat the copper surface shown in figure 1, while S_{CG} refers to continuous graphene domains that link together and fully cover the copper surface shown in figure 3. Besides two typical peaks representing Cu2p$_{3/2}$ ($\sim$952.4 eV) and Cu 2p$_{1/2}$ ($\sim$932.5 eV), a Cu^{2+} peak ($\sim$944.1 eV) in figure 2(c) is found more strongly in the S_{IG} sample, indicating higher oxidizing degree. Accordingly, the C 1s curve of sample S_{IG} in

figure 2(d) demonstrates a decreased C–C peak ($\sim$284.5 eV) and the appearance of a minor C=O peak ($\sim$288.0 eV), which further verifies that the uncoated copper is more easily oxidized. Regarding the appearance of the C=O signal, we attribute it to the oxidation process of unsaturated carbon atoms on domain boundaries of sample S_{IG}. Due to the tight connection among boundaries, the unsaturated carbon atoms are much fewer in sample S_{CG} than in S_{IG} and the C=O signal did not exist in sample S_{CG}. The atomic percentage of oxygen in S_{CG} is 3.3%, which is far less than the 28.7% in S_{IG}. We concluded that the inducing oxygen leads to a darker contrast of the copper substrate. It is worth noting that the SE contrasts of the graphene edges are deeper in figure 2(a) than those in other previous work [33, 41]. We investigated the oxidation process by observing sample S_{IG} through different modes exposed after one month in air, shown in figures 2(e) and (f), respectively. With increase in exposure time, copper oxidation continued to occur at the interface between the copper surface and the graphene domains. The contrast difference on the edge of the mono-layer graphene region is becoming larger in figure 2(e). From the corresponding mixed SE/BSE mode image shown in figure 2(f), the darker contrast on the edges of the graphene extendd from the edges to the centers of the graphene domains. As a result, the graphene domains cannot be seen in detail since the contrast converges, leaving only graphene domain borders visible. It is known that graphene maintains a continuous structure over terraces and ledges of the copper surface [32]. However, oxygen gas can gradually enter through border between the graphene and the copper, and spread along the copper ledges reacting with the copper, from the edge of the graphene into the center region. The result visualized in the SEM image is coincident with the work carried out previously [4]. In conclusion, graphene can greatly delay the oxidation process on the copper surface.

In contrast to sample S_{IG}, continuous graphene sample S_{CG} exhibits the different images shown in figure 3. Figures 3(a) and (b) show images taken by SEM through the different modes. We chose images with several residue particles to demonstrate the same region. Like figure 1, the few-layer part of the graphene domain cannot be seen in the SE mode image shown in figure 3(a), while it is clearly seen layer by layer in figure 3(b) by adding BSE signals. The former darker contrast representing the copper substrate disappears. The Raman spectra of point A in figure 3(b) exhibit the mono-layer curve shown in figure 3(d), indicating that the lightest contrast in the large continuous areas represents mono-layer graphene. Moreover, the graphene domain at the point B region in figure 3(b) is verified to be of the few-layer type, as demonstrated by the other Raman curve in figure 3(d). However, the Raman mapping technique is low in resolution due to its large spot size which is unable to precisely verify our assumption. Figure 3(c) illustrates the average contrast difference between two mode images of a continuous graphene film grown on copper. The curves demonstrate the great difference between the two modes. The contrast is almost the same among different graphene layers using the SE signal, but shows a significant slope under the mixed signal mode. The contrast difference of the adjacent
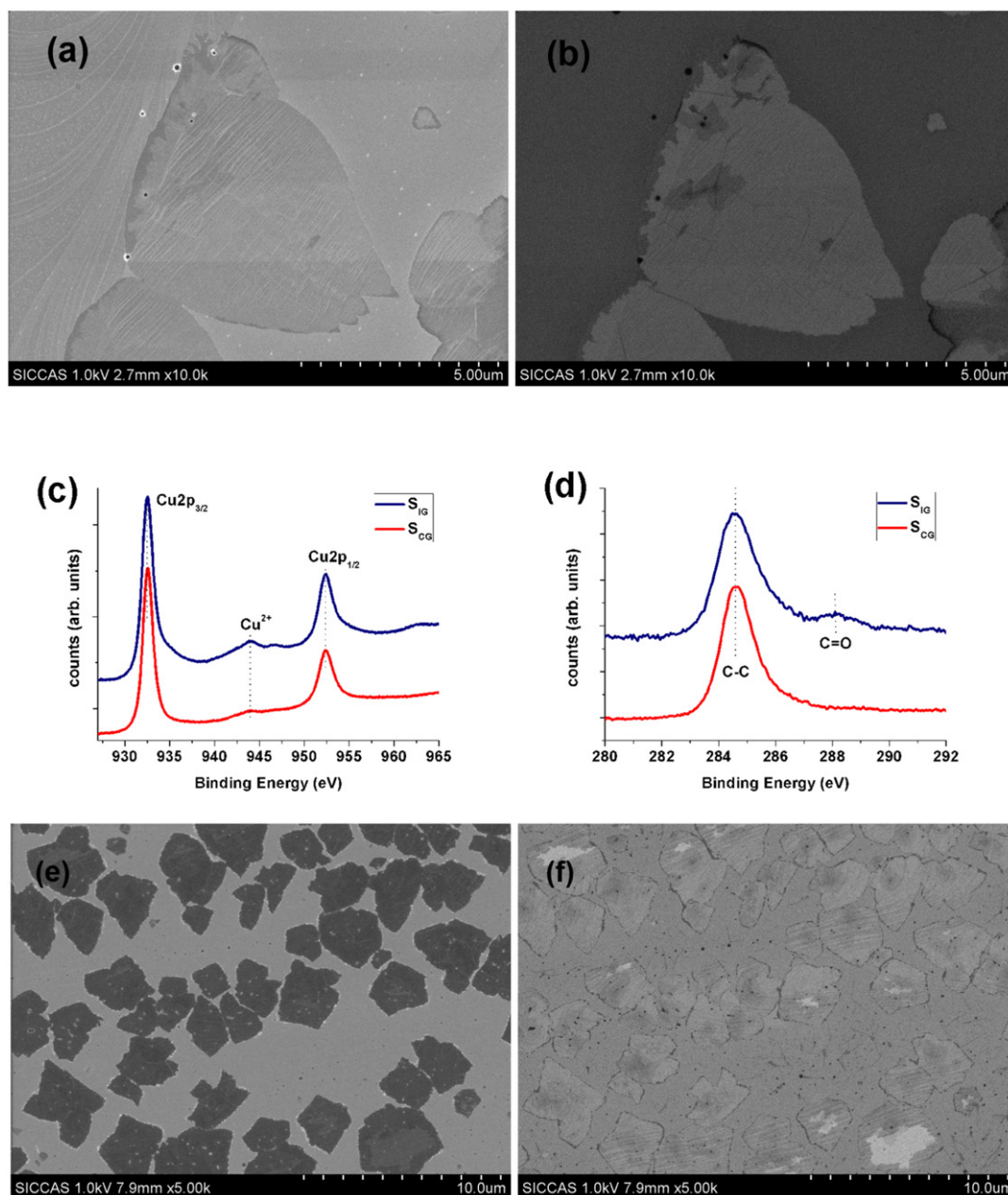
Figure 2. SEM images of isolated graphene domains of (a), (e) the SE mode and (b), (f) the mixed SE/BSE mode. Parts (c) and (d) illustrate XPS curves of copper and carbon peaks using S_{IG} and S_{CG}.

layer is ∼8%. This comparison further proves that the method we have developed is facile for observing the number of graphene layers. Also, the formation of mono-layer graphene wrinkles can be seen more easily in the mixed SE/BSE mode than in the SE mode. The graphene wrinkles have the same contrast as the third-layer graphene, further demonstrating the single-layer nature of the continuous graphene. It is important to mention that the difference between the wrinkles and the oxidized copper region is that the wrinkles do not spread along the copper ledges, as seen in figure 2. Meanwhile the SE mode image of figure 3(a) shows a clearer terrace–ledge structure (TL structure). Therefore, through combining the SE mode and SE/BSE mixed mode SEM observation, it will be easier to investigate the relationship between the graphene

growth tendency and uniformity with the copper substrate microstructures.

Extensive studies [2, 10] have been made to get a better understanding of the mechanisms of graphene growth by the CVD method at the microlevel, while few have concentrated on the relative macrolevel. The catalyst structure is important for high-quality graphene growth. Possessing the advantage of very low carbon solubility and strength of the stable filled 3d-electron shell [28], copper seems to be an ideal catalyst for CVD graphene growth, as was discovered in 2009 [21]. Recent investigations [39] have reported that the diverse surface facets of the polycrystalline copper substrate affect the graphene growth. However, the weird phenomenon of growth in a linear row distribution [35] of graphene domains
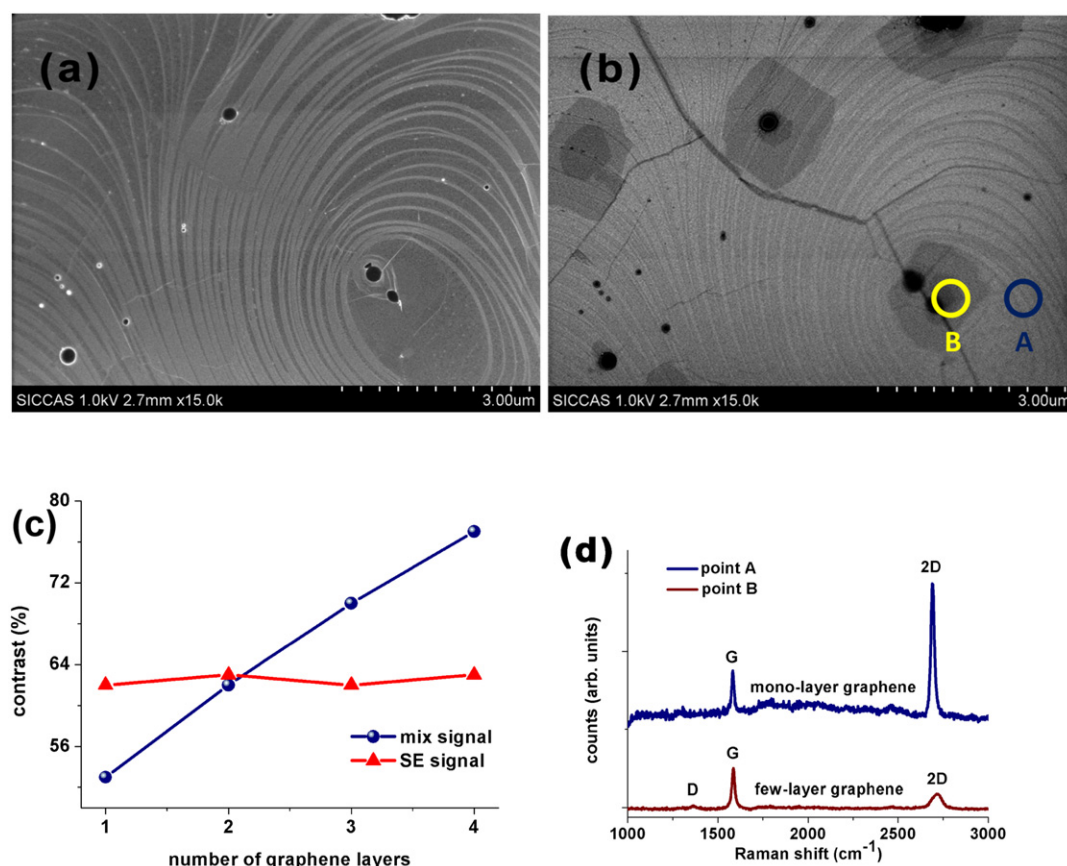
Figure 3. SEM images of continuous few-layer graphene domains of (a) the SE mode and (b) the mixed SE/BSE mode. (c) Illustrates curves of average contrast difference between two mode images. (d) Exhibits Raman spectra for the indicated regions of the graphene domain in (b).

on copper foil has not been explained so far. An earlier experiment described that although the flat surface of a copper substrate was scratched, lines of graphene domains could be obtained [12]. The uneven surface structure of raw rolled copper foil may affect graphene growth. Figures 4(a) and (c) show SEM images of raw copper foil and copper foil after a 20 min annealing process, respectively. For reference, images of the same material taken by an optical microscope (OM) whose depth of field was limited are shown in figures 4(b) and (d), respectively. It is seen in figure 4(c) that the surface of the copper was reconstructed, as seen in the macroscopic view of SEM. However, the original morphology of the rolled copper foil with linear peaks and valleys was not changed during annealing process, as illustrated in figures 4(b) and (d). The TL structure is easily obtained on the copper surface under hydrogen atmosphere at high temperatures [17, 37] with a large number of unsaturated copper atoms. Dense ledges possess more unsaturated copper atoms than terraces. It has been previously simulated [10] that the nucleation barrier near ledges is lower than on terraces. The graphene domains grow in aligned rows whose direction is the same as that of the copper [35]. Since graphene can protect the TL structure of copper, we chose sample S_{CG} to investigate the relationship between the unevenness of the copper and the graphene growth tendency.

Figures 5(a) and (b) exhibit images of sample S_{CG} by SE mode and mixed SE/BSE mode SEM, respectively. It is obvious in figure 5(a) that the whole surface TL structure of the copper foil was preserved by the continuous covering of graphene. Figure 5(b) illustrates the distribution of graphene domains by the location of few-layer graphene parts since the few-layer graphene regions represent nucleation sites. By comparing the two SEM images with different modes, we found that linearly grown few-layer graphene domains are distributed on regions with more concentrated ledges, while mono-layer graphene on flatter regions with more terraces. This is in accordance with previous reports. However, the surface unevenness of the copper can hardly be seen in the SEM images discussed in figure 4, so we took OM images which have a much shallower field depth, as shown in figure 5(c). Through another comparison between figures 5(a) and (c), we find that the surface unevenness of the copper foil induced an inhomogeneous linear array distribution of ledges. Dense ledges are distributed in the slope regions while terraces are located in flat regions. Through the observation above, a schematic diagram illustrating details of the surface copper structure is presented in figure 5(d). The red region is the flat valley and the peak part where ledges are fewer. The flat positions are suitable for a fast surface adsorption progress which leads to mono-layer graphene growth. On the other hand, the blue region is the copper slope with dense
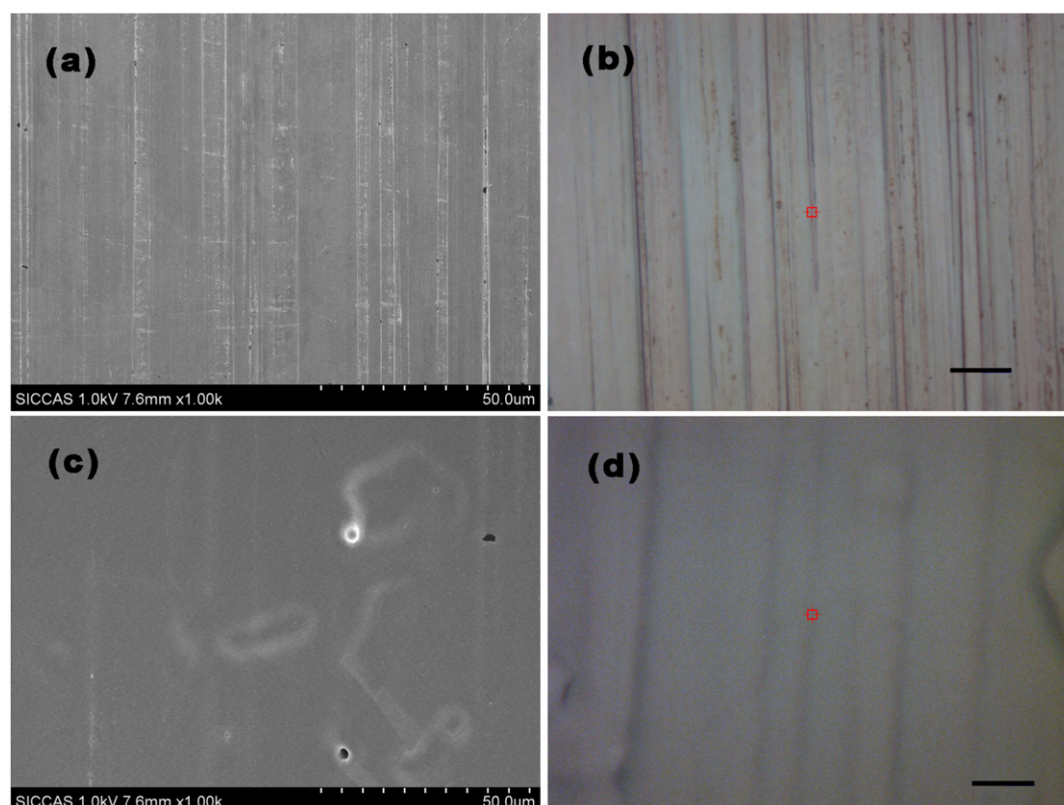
Figure 4. SEM images of copper (a) before and (c) after annealing. OM images of copper (b) before and (d) after annealing (scale bar 10 μm).

ledges which served as graphene nucleation sites. Because of the nature of the copper foil, these ledge regions formed in linear rows and thus led to the same distribution of graphene domains. This result explains the formation of linear graphene domains [2, 35] and accords with theoretical results [10]. The above results indicate that the uneven surface of the copper foil after annealing strongly affects graphene domain growth. Besides the surface unevenness, residue particles act as nucleation sites which can also lower the formation energy of graphene.

In summary, we concluded on the growth mechanism of few-layer graphene growth on copper foil. Both surface adsorption and epitaxial growth deposition processes exist under these circumstances. However, the speed of epitaxial graphene growth is much lower than the surface adsorption process due to different barriers. Mono-layer graphene grows rapidly on terrace regions. When the copper substrate is fully covered with graphene and surface adsorption stops, the deposition process continues and carbon islands are formed. Thus, the growth of graphene domains does not follow the two-dimensional Frank–van der Merwe thin-film growth mode [29]. Under atmospheric conditions, the Stranski–Krastanov growth mode [29] is probably suitable for explaining the growth process which is an intermediary process characterized by both 2D layer and 3D island growth. At first 2D layer growth prevails. When the 2D layer totally covers the copper foil, 3D island growth continues. This growth mode is highly dependent on the

chemical and physical properties, such as surface energies and lattice parameters of the substrate and the graphene. We verified that by increasing the growing time to 10 min we obtained more inhomogeneous graphene domains, as shown in figure S5 of the supporting information (available at stacks.iop.org/Nano/23/475705/mmedia). To the best of our knowledge, no large-area homogeneous bi-layer graphene film has been synthesized on copper until now. Recently Liu and his colleagues [40] presented layer-by-layer epitaxial bi-layer Bernal graphene on copper and obtained a 67% coverage of bi-layer graphene regions. However, there is still a distance to large-area homogeneous graphene production. In our opinion, according to the characterization and analysis discussed above, thicker graphene layer growth on copper foil is limited by the migration energy of carbon on a graphene substrate. Large-area bi-layer graphene can hardly be obtained on copper foil. The obtained inhomogeneous graphene is transferred [1, 25, 26] to PET substrates. The surface resistance of the transparent conductive film is $R_\mathrm{s} = 1000\ \Omega/\square$ with a transparency of 96% at 550 nm without further optimization such as decreasing the carbon source proportion [2], improving the vacuum [23] or chemical mechanical polishing of the copper [12]. Since the intensity of the D peak is small in most regions except edges, we attribute the resistance to a large number of nucleation points which increase the contact length among domains [16]. The loss of transparency is caused by the upper graphene layers which did not link together and thus barely contributed to the conductivity.
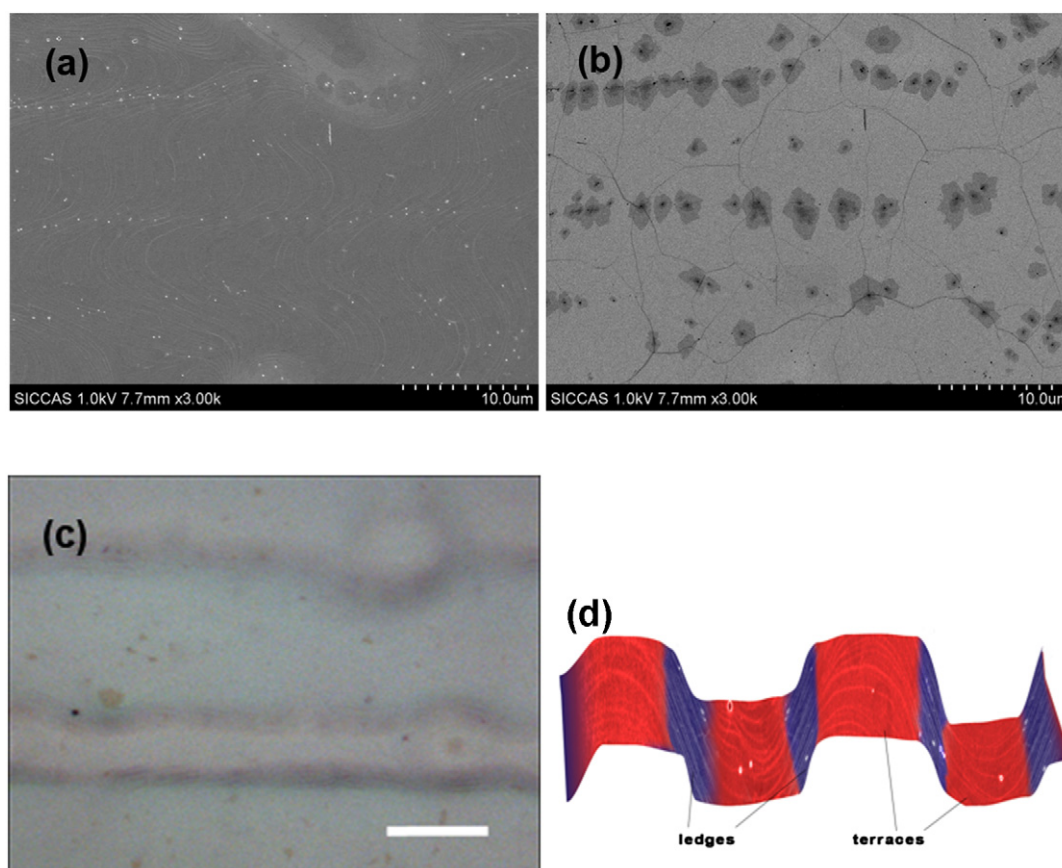
Figure 5. Continuous few-layer graphene domains by (a) SE mode and (b) mixed SE/BSE mode SEM images and (c) OM image (scale bar 10 μm). (d) Schematic diagram illustrating details of the surface copper structure.

4. Conclusion

We present a SEM method where both SE and BSE signals are collected to observe graphene clearly with distinct contrast representing each layer of a pyramidal domain. This method provides an efficient way of checking the uniformity of graphene film on copper and other catalysts. We studied the contrast difference representation of different substances and the slow oxidation process from the edge to inside the graphene domain. Furthermore, through SEM and Raman techniques, we firstly investigated the relationship between the graphene domain growth tendency and the surface unevenness of the rolled copper foil. Combining theoretical results reported before and our experimental results, we concluded that the nucleation and growth speed of the graphene domains depends on the distributions of ledges and terraces on the copper. Our results explain the formation of linear graphene domains and accord with theoretical results.

References

[1] Bae S *et al* 2010 Roll-to-roll production of 30-inch graphene films for transparent electrodes *Nature Nanotechnol.* **5** 574–8

[2] Bhaviripudi S, Jia X T, Dresselhaus M S and Kong J 2010 Role of kinetic factors in chemical vapor deposition synthesis of uniform large area graphene using copper catalyst *Nano Lett.* **10** 4128–33

[3] Castro Neto A H, Guinea F, Peres N M R, Novoselov K S and Geim A K 2009 The electronic properties of graphene *Rev. Mod. Phys.* **81** 109–62

[4] Chen S S *et al* 2011 Oxidation resistance of graphene-coated Cu and Cu/Ni alloy *ACS Nano* **5** 1321–7

[5] Chen S S, Cai W W, Piner R D, Suk J W, Wu Y P, Ren Y J, Kang J Y and Ruoff R S 2011 Synthesis and characterization of large-area graphene and graphite films on commercial Cu–Ni alloy foils *Nano Lett.* **11** 3519–25

[6] de Heer W A *et al* 2007 Epitaxial graphene *Solid State Commun.* **143** 92–100

[7] Dresselhaus M S, Jorio A, Hofmann M, Dresselhaus G and Saito R 2010 Perspectives on carbon nanotubes and graphene Raman spectroscopy *Nano Lett.* **10** 751–8

[8] Farrow R F C 1987 *Thin Film Growth Techniques for Low-Dimensional Structures* (New York: Plenum)

[9] Ferrari A C *et al* 2006 Raman spectrum of graphene and graphene layers *Phys. Rev. Lett.* **97** 187401

[10] Gao J F, Yip J, Zhao J J, Yakobson B I and Ding F 2011 Graphene nucleation on transition metal surface: structure transformation and role of the metal step edge *J. Am. Chem. Soc.* **133** 5009–15

[11] Goldstein J 2003 *Scanning Electron Microscopy and X-ray Microanalysis* (New York: Kluwer, Academic, Plenum)

[12] Han G H, Gunes F, Bae J J, Kim E S, Chae S J, Shin H-J, Choi J-Y, Pribat D and Lee Y H 2011 Influence of copper morphology in forming nucleation seeds for graphene growth *Nano Lett.* **11** 4144–8

[13] Hernandez Y *et al* 2008 High-yield production of graphene by liquid-phase exfoliation of graphite *Nature Nanotechnol.* **3** 563–8

[14] Hesjedal T 2011 Continuous roll-to-roll growth of graphene films by chemical vapor deposition *Appl. Phys. Lett.* **98** 133106

[15] Hiura H, Miyazaki H and Tsukagoshi K 2010 Determination of the number of graphene layers: discrete distribution of the secondary electron intensity stemming from individual graphene layers *Appl. Phys. Express* **3** 095101

[16] Jeong C W, Nair P, Khan M, Lundstrom M and Alam M A 2011 Prospects for nanowire-doped polycrystalline graphene films for ultratransparent, highly conductive electrodes *Nano Lett.* **11** 5020–5

[17] Ji H X *et al* 2011 Graphene growth using a solid carbon feedstock and hydrogen *Acs Nano* **5** 7656–61

[18] Kim J, Kim F and Huang J X 2010 Seeing graphene-based sheets *Mater. Today* **13** 28–38

[19] Kim K S, Zhao Y, Jang H, Lee S Y, Kim J M, Ahn J H, Kim P, Choi J Y and Hong B H 2009 Large-scale pattern growth of graphene films for stretchable transparent electrodes *Nature* **457** 706–10

[20] Kochat V, Pal A N, Sneha E S, Sampathkumar A, Gairola A, Shivashankar S A, Raghavan S and Ghosh A 2011 High contrast imaging and thickness determination of graphene with in-column secondary electron microscopy *J. Appl. Phys.* **110** 014315

[21] Li X S *et al* 2009 Large-area synthesis of high-quality and uniform graphene films on copper foils *Science* **324** 1312–4

[22] Li X S, Cai W W, Colombo L and Ruoff R S 2009 Evolution of graphene growth on Ni and Cu by carbon isotope labeling *Nano Lett.* **9** 4268–72

[23] Li X S *et al* 2010 Graphene films with large domain size by a two-step chemical vapor deposition process *Nano Lett.* **10** 4328–34

[24] Li X S, Magnuson C W, Venugopal A, Tromp R M, Hannon J B, Vogel E M, Colombo L and Ruoff R S 2011 Large-area graphene single crystals grown by low-pressure chemical vapor deposition of methane on copper *J. Am. Chem. Soc.* **133** 2816–9

[25] Li X S, Zhu Y W, Cai W W, Borysiak M, Han B Y, Chen D, Piner R D, Colombo L and Ruoff R S 2009 Transfer of large-area graphene films for high-performance transparent conductive electrodes *Nano Lett.* **9** 4359–63

[26] Liang X L *et al* 2011 Toward clean and crackless transfer of graphene *ACS Nano* **5** 9144–53

[27] Liu N, Fu L, Dai B Y, Yan K, Liu X, Zhao R Q, Zhang Y F and Liu Z F 2011 Universal segregation growth approach to wafer-size graphene from non-noble metals *Nano Lett.* **11** 297–303

[28] Mattevi C, Kim H and Chhowalla M 2011 A review of chemical vapour deposition of graphene on copper *J. Mater. Chem.* **21** 3324–34

[29] Wu Z Q 2001 *Thin Film Growth* (Beijing: Science Press)

[30] Novoselov K S, Geim A K, Morozov S V, Jiang D, Zhang Y, Dubonos S V, Grigorieva I V and Firsov A A 2004 Electric field effect in atomically thin carbon films *Science* **306** 666–9

[31] Park S and Ruoff R S 2009 Chemical methods for the production of graphenes *Nature Nanotechnol.* **4** 217–24

[32] Rasool H I, Song E B, Allen M J, Wassei J K, Kaner R B, Wang K L, Weiller B H and Gimzewski J K 2011 Continuity of graphene on polycrystalline copper *Nano Lett.* **11** 251–6

[33] Rasool H I, Song E B, Mecklenburg M, Regan B C, Wang K L, Weiller B H and Gimzewski J K 2011 Atomic-scale characterization of graphene grown on copper (100) single crystals *J. Am. Chem. Soc.* **133** 12536–43

[34] Reimer L 1998 *Scanning Electron Microscopy: Physics of Image Formation and Microanalysis* (Berlin: Springer)

[35] Robertson A W and Warner J H 2011 Hexagonal single crystal domains of few-layer graphene on copper foils *Nano Lett.* **11** 1182–9

[36] Sun Z Z, Yan Z, Yao J, Beitler E, Zhu Y and Tour J M 2010 Growth of graphene from solid carbon sources *Nature* **468** 549–52

[37] Vlassiouk I, Regmi M, Fulvio P, Dai S, Datskos P, Eres G and Smirnov S 2011 Role of hydrogen in chemical vapor deposition growth of large single-crystal graphene *ACS Nano* **5** 6069–76

[38] Wang X R, Ouyang Y J, Li X L, Wang H L, Guo J and Dai H J 2008 Room-temperature all-semiconducting sub-10 nm graphene nanoribbon field-effect transistors *Phys. Rev. Lett.* **100** 206803

[39] Wood J D, Schmucker S W, Lyons A S, Pop E and Lyding J W 2011 Effects of polycrystalline CU substrate on graphene growth by chemical vapor deposition *Nano Lett.* **11** 4547–54

[40] Yan K, Peng H, Zhou Y, Li H and Liu Z 2011 Formation of bilayer bernal graphene: layer-by-layer epitaxy via chemical vapor deposition *Nano Lett.* **11** 1106–10

[41] Yu Q *et al* 2011 Control and characterization of individual grains and grain boundaries in graphene grown by chemical vapour deposition *Nature Mater.* **10** 443–9